Evolutionary Models of Convergent Margins : Origin of Their Diversity

Fission Track Thermochronology of Late Cretaceous Sandstones of the Izumi Group Adjacent to the Median Tectonic Line Active Fault System in Southwest Japan

Yasuto Itoh, Paul F. Green, Keiji Takemura and
Tomotaka Iwata

Additional information is available at the end of the chapter

Abstract

Fission track (FT) thermochronology was applied to the Late Cretaceous turbidite sandstones of the Izumi Group adjacent to the Median Tectonic Line active fault system in southwest Japan. Apatite FT analyses revealed the following three stages of cooling (uplift) events: 95–78 Ma (Cenomanian–Campanian) from >130°C, 74–46 Ma (Campanian–middle Eocene) from approximately 100°C, and 27–7 Ma (late Oligocene–late Miocene) from approximately 70°C. By contrast, zircon FT analysis indicated cooling from >300°C at ca. 70 Ma. Apparent discrepancies between the cooling initiation times obtained using the two analytical methods indicate the distinct provenances of tuffaceous sandstones of the Izumi Group. The second episode is likely related to regional exhumation events on the eastern Eurasian margin. The latest event, which terminated by the end of the Miocene, appears to have been manifested in the strong deformation of the arc under a compressive stress provoked by the resumed subduction of the Philippine Sea Plate.

Keywords: fission track, thermochronology, Cretaceous, Izumi Group, southwest Japan

1. Introduction

Reflecting transient shifts in the convergence modes of oceanic plates, island arcs are sites of complicated deformation events, which provide insight into the timeline of plate motions. Although such tectonic records can be obtained as temporal changes in the sedimentary environments in basin areas, the deformation history of exhumed terranes is difficult to assess because of a lack of direct evidence. This paper presents a case study of fission track thermo-

chronology of the Late Cretaceous sandstones of the Izumi Group that constitute a mountain range along a longstanding crustal break called the Median Tectonic Line (MTL) on the eastern Eurasian convergent margin. The present study provides the first-ever quantitative information on recurrent uplifts of the southwestern Japan arc, which was a part of the continental rim before the Neogene backarc rifting.

2. Geological background

During the Cretaceous, the MTL acted as a sinistral transcurrent fault along the eastern Eurasian margin [1]. As a result of repeated slips on the fault and the propagation of its termination, an enormous narrow pull-apart basin was generated with the eastward migration of the depocenter. The present study was focused on the easternmost part of the basin, which was buried with the Maastrichtian marine sediments of the Izumi Group [2].

A sedimentological study [3] has shown that the Izumi Group basically consists of stacks of mega-units. Facies associations indicate that the constituents of the units are classified into the depositional systems including main channels with overspilled deposits, distributary channels, and sheet flows.

Outcrop sandstone samples of the Izumi Group were obtained from two sites on a reservoir (**Figure 1**). Sp. 15040401 was taken on the surface of a reverse fault (within 30 cm) called the Negoro–Minami Fault, whose Quaternary movement has been confirmed [2]. Sp. 15040402 was taken from a site at least 60 m from the same fault.
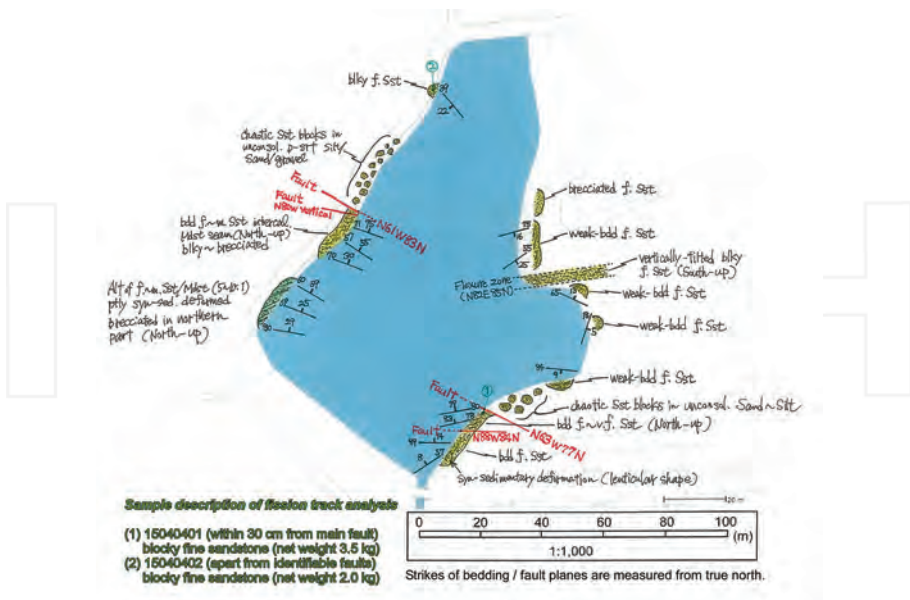

Figure 1. Sampling locality map. See the prologue of this section for the regional index.

3. Analytical methods and results

In this chapter, the authors provide new Apatite Fission Track Analysis (AFTA®) and Zircon Fission Track Analysis (ZFTA™) data and the associated thermal history interpretations for two samples of outcropping Maastrichtian sandstones from southwest Japan. AFTA and ZFTA results have been used to identify, characterize, and quantify the main heating and cooling episodes that have affected the section from which the samples were taken. This information was then synthesized to provide a regionally consistent thermal history framework, from which the history of the structural and tectonic development at the sample location can be understood.

3.1. Sample preparation

Outcrop samples were crushed in a jaw crusher and then ground to sand grade in a rotary disc mill. The ground samples were rinsed to remove dust, then dried, and processed by the conventional mineral separation techniques, namely heavy liquid and magnetic separator in order to obtain heavy minerals. Acquired apatite grains were mounted in epoxy resin sheet set on hot glass slides. It was polished to reveal internal crystal surfaces and etched for 20 s in 5 M HNO_3 in room temperature (20°C) for visualization of spontaneous fission tracks. Zircon grains were embedded in FEP Teflon sheet between heated microscope slides on a hot plate, polished to expose internal surfaces, and then etched in a molten KOH:NaOH eutectic etchant at ~220°C, for an appropriate time (usually 10–100 h) to reveal properly etched fission tracks contained in a high proportion of the grains.

After the etching procedure, all mounts were cut to 1.5×1.0 cm, and soaked in detergent, alcohol, and distilled water to clean them up. They were sealed in close contact with low-uranium detectors made of muscovite wrapped within heat-shrink membrane. Each batch of mounted samples was stacked between two pieces of uranium standard glass prepared in a similar fashion. It was then settled in an aluminum can for irradiation.

After neutron irradiation, mica detectors were removed from the mounted grains and standard glasses, and then etched in hydrofluoric acid to visualize the induced fission tracks produced by ^{235}U inherently contained in the apatite/zircon and standard glass.

3.2. Data quality

Excellent apatite yields were obtained from the two samples (**Table 1**), with fission track ages in 20 or more grains and 100 track lengths or more measured (the usual "target" numbers considered necessary for an analysis of the highest quality) in both samples. The apatite grains that were analyzed in both samples were of high quality. Thus, high-quality data were obtained for both samples, and the resulting thermal history constraints are regarded as highly reliable.

Both samples provided excellent yields of detrital zircon, with 20 single grain ages measured in both samples, resulting in very high-quality data. As with the apatites, the quality of the polished and etched surfaces in all analyzed zircon grains was high, and the resulting data are of very high quality.

Sample no. (ID in paper)	Loc. (lat./long.)	Lithology (remarks)	Stratigraphic division	Strat. age (Ma)	Raw wt. (g)	Washed wt. (g)	Apatite yield*
GC1181-3 (15040401)	34.2800/135.3100	Mass. f. sandstone (adjacent to fault)	Izumi Group (Maastrichtian)	71–65	2420	310	Excellent
GC1181-4 (15040402)	34.2800/135.3100	Mass. f. sandstone (apart from fault)	Izumi Group (Maastrichtian)	71–65	2040	360	Excellent

* Yield is based on the quantity of mineral separates which suit age determination. Excellent: >20 grains; good: 15–19 grains; fair: 10–14 grains; poor: 5–9 grains; very poor: <5 grains.

Table 1. Details of fission track samples and apatite yields.

3.3. Fission track ages

Fission track ages were calculated using the standard fission track age equation with the zeta calibration method (Eq. (5) of [4]). We determined ages by means of the external detector method (EDM; [5]). The EDM has a merit that fission track ages can be determined for single grains. In case of apatite, tracks are counted for each mount in 20 grains. If the desired number is not present in those samples, all available grains are counted. The actual number depends on the availability of suitably etched and oriented grains. We exclusively analyzed grains oriented with surfaces parallel to the crystallographic c-axis. Such grains are found based on etching characteristics, together with morphological evidence within euhedral grains. The grain mount is then sequentially scanned, and the first-identified 20 suitably oriented grains are treated by following procedures.

We count tracks within an eyepiece graticule that is divided into 100 grid squares. The number of spontaneous tracks (N_s) within a certain number of grid squares (N_a) was recorded in each grain. Then, we count the number of induced tracks (N_i) in the corresponding location of the external detector made of mica. Densities of spontaneous and induced tracks (ρ_s and ρ_i) are calculated by dividing the track counts by the total area counted, which is determined as the product of N_a and the area or each grid square. Eventually, fission track ages are calculated by substituting track counts (N_s and N_i) for track densities (ρ_s and ρ_i).

We carried out neutron irradiations in a well-thermalized flux (X-7 facility; Cd ratio for Au ~98) in the research reactor HIFAR of Australian Atomic Energy Commission. Track counts in mica external detectors attached to two pieces of Corning Glass Works standard glass CN5 (containing ~11 ppm Uranium) in the irradiation canister at each end of the sample stack provided us with total neutron fluence. Twenty-five fields were normally counted in each detector to determine track densities within external detectors irradiated adjacent to uranium standard glasses. The track density (ρ_D) was determined when we divided the total track count (N_D) by the total area counted. Covering the whole area of the detector, positions of the counted fields were arranged in a 5 × 5 grid. This is convenient to sample across the detector while gathering sufficient counts for the achievement of a precision of ~±2% within a reasonable time for typical track densities between approximately 5×10^5 and 5×10^6.

In the irradiation facility described above, small flux gradient is often observed over the length of the sample package. In case a detectable gradient is present, we convert the track count in the external detector adjacent to each standard glass to a track density (ρ_D), and a value for

each mount in the stack is estimated based on linear interpolation. Or else, when no significant gradient is detected, we pool the track counts in the two external detectors to give a single value of ρ_D, based on which fission track ages for each sample are calculated. Detailed information of the apatite dating is given in **Tables 2** and **3** for Sp. 15040401 and 15040402, respectively.

GC1181-3 Apatite										15040401
Counted by: MEM										
Slide ref	Current grain no	N_s	N_i	N_a	ρ_s	ρ_i	RATIO	U (ppm)	Cl (wt%)	F.T. AGE (Ma)
G1264-2	3	3	10	36	1.324E+05	4.414E+05	0.300	3.8	0.35	78.3 ± 51.6
G1264-2	5	12	55	100	1.907E+05	8.740E+05	0.218	7.5	0.86	57.1 ± 18.3
G1264-2	6	8	27	56	2.270E+05	7.662E+05	0.296	6.5	0.94	77.4 ± 31.2
G1264-2	7	25	127	60	6.621E+05	3.364E+06	0.197	28.7	0.23	51.5 ± 11.4
G1264-2	8	5	34	60	1.324E+05	9.005E+05	0.147	7.7	0.22	38.5 ± 18.5
G1264-2	9	5	20	40	1.986E+05	7.945E+05	0.250	6.8	0.10	65.3 ± 32.7
G1264-2	11	3	9	32	1.490E+05	4.469E+05	0.333	3.8	0.97	87.0 ± 58.0
G1264-2	12	8	41	100	1.271E+05	6.515E+05	0.195	5.6	0.83	51.0 ± 19.8
G1264-2	14	9	9	32	4.469E+05	4.469E+05	1.000	3.8	0.29	257.5 ± 121.6
G1264-2	17	2	10	36	8.828E+04	4.414E+05	0.200	3.8	0.22	52.3 ± 40.6
G1264-2	18	7	17	64	1.738E+05	4.221E+05	0.412	3.6	0.97	107.3 ± 48.3
G1264-2	19	23	123	30	1.218E+06	6.515E+06	0.187	55.5	0.21	48.9 ± 11.2
G1264-2	22	8	16	70	1.816E+05	3.632E+05	0.500	3.1	0.44	130.0 ± 56.4
G1264-2	23	9	30	70	2.043E+05	6.810E+05	0.300	5.8	0.90	78.3 ± 29.9
G1264-2	25	16	38	49	5.189E+05	1.232E+06	0.421	10.5	0.09	109.7 ± 32.8
G1264-2	26	22	79	49	7.135E+05	2.562E+06	0.278	21.8	0.09	72.7 ± 17.7
G1264-2	27	13	61	100	2.066E+05	9.693 E+05	0.213	8.3	0.90	55.7 ± 17.1
G1264-2	29	7	29	49	2.270E+05	9.405E+05	0.241	8.0	1.00	63.1 ± 26.6
G1264-2	30	7	21	30	3.708E+05	1.112E+06	0.333	9.5	0.92	87.0 ± 38.0
G1264-2	33	0	5	36	0.000E+05	2.207E+05	0.000	1.9	0.30	0.0 ± 106.0
		192	761		2.776E+05	1.100E+06		9.4		

Area of basic unit = 6.293E-07 cm⁻² Ages calculated using a zeta of 392.9 ± 7.4 for CN5 glass

χ^2 = 24.656 with 19 degrees of freedom ρ = 1.337E+06cm⁻² ND =2212

$P(\chi^2)$ = 17.2% ρ_D interpolated between the top of can; ρ = 1.328E+06cm⁻² ND = 1045

Age Dispersion = 11.181% (did not converge} bottom of can; ρ = 1.484E+06cm⁻² ND = 1167

N_s/N_i =0.252 ± 0.020 **POOLED AGE = 65.9 ± 5.6 Ma**

Mean Ratio= 0.301 ± 0.044 CENTRAL AGE = 67.0 ±6.1 Ma

Table 2. Details of apatite fission track analysis for Sp. 15040401.

GC1181-4 Apatite									**15040402**	
Counted by: MEM										
Slide ref	Current grain no	N_s	N_i	N_a	ρ_s	ρ_i	RATIO	U (ppm)	Cl (wt%)	F.T. AGE (Ma)
G1264-3	3	6	12	30	3.178E+05	6.356E+05	0.500	5.4	0.87	130.8 ± 65.5
G1264-3	5	2	13	42	7.567E+04	4.919E+05	0.154	4.2	0.95	40.5 ± 30.8
G1264-3	6	8	10	40	3.178E+05	3.973E+05	0.800	3.4	0.91	208.1 ± 98.9
G1264-3	7	6	29	50	1.907E+05	9.217E+05	0.207	7.8	0.77	54.5 ± 24.5
G1264-3	8	7	19	42	2.648E+05	7.189E+05	0.368	6.1	0.85	96.7 ± 42.8
G1264-3	10	12	50	70	2.724E+05	1.135E+06	0.240	9.6	0.89	63.1 ± 20.4
G1264-3	11	7	21	80	1.390E+05	4.171E+05	0.333	3.5	0.28	87.5 ± 38.3
G1264-3	12	2	12	60	5.297E+04	3.178E+05	0.167	2.7	0.47	43.9 ± 33.6
G1264-3	13	1	11	24	6.621E+04	7.283E+05	0.091	6.2	0.61	24.0 ± 25.1
G1264-3	14	10	21	42	3.783E+05	7.945E+05	0.476	6.7	1.07	124.7 ± 48.0
G1264-3	15	14	43	70	3.178E+05	9.761 E+05	0.326	8.3	0.36	85.5 ± 26.4
G1264-3	16	1	14	60	2.648E+04	3.708E+05	0.071	3.1	0.71	18.9 ± 19.5
G1264-3	20	1	6	30	5.297E+04	3.178E+05	0.167	2.7	0.26	43.9 ± 47.4
G1264-3	21	7	25	35	3.178E+05	1.135E+06	0.280	9.6	1.02	73.6 ± 31.5
G1264-3	22	9	19	49	2.919E+05	6.162E+05	0.474	5.2	1.04	124.0 ± 50.3
G1264-3	26	10	33	80	1.986E+05	6.555E+05	0.303	5.6	0.90	79.6 ± 28.8
G1264-3	27	7	19	36	3.090E+05	8.387E+05	0.368	7.1	0.88	96.7 ± 42.8
G1264-3	28	10	25	100	1.589E+05	3.973E+05	0.400	3.4	0.91	104.9 ± 39.4
G1264-3	33	8	39	64	1.986E+05	9.683E+05	0.205	8.2	0.87	54.0 ± 21.0
G1264-3	34	14	27	25	8.899E+05	1.716E+06	0.519	14.5	0.59	135.6 ± 44.8
G1264-3	79	9	21	36	3.973E+05	9.270E+05	0.429	7.9	0.98	112.3 ± 44.9
		151	469		2.253 E+05	6.998E+05		5.9		

Area of basic unit = 6.293E-07 cm^{-2}

Ages calculated using a zeta of 392.9 + 7.4 for CN5 glass

χ^2 = 19.588 with 20 degrees of freedom

ρ =1.346E+06cm^{-2} ND=2212

$P(\chi^2)$=48.4%

ρ_D interpolated between the top of can; ρ = 1.328E+06cm^{-2} ND = 1045

Age dispersion =2.735% (did not converge)

bottom of can; ρ = 1.484E+06^{-2} ND = 1167

N_s/N_i= 0.322 ± 0.030

POOLED AGE = 84.6 ± 8.3 Ma

Mean ratio = 0.327 ± 0.038

CENTRAL AGE = 84.6 ± 8.3 Ma

Table 3. Details of apatite fission track analysis for Sp. 15040402.

3.4. Track length measurements

Applications of fission track dating to accessory apatites from crystalline basement rocks revealed that the technique was extremely thermally sensitive, suggesting that fission track ages could be reset at relatively low temperatures around 100°C over geological timescales (e.g. [6]). This was confirmed by the direct measurement of fission track ages in subsurface samples [7]. Integration of fission track ages with confined track length measurements [8] led to deeper understanding of the method. Early measurements showed that even in volcanic rocks, which have experienced only very low temperatures after initial post-eruption cooling, the mean confined track lengths (around 14–15 µm) were shorter than the induced tracks (~16 µm) in the same apatites. Green [9] showed that this can be understood in terms of the thermal annealing of these tracks at low temperatures (<50°C) over geological timescales, highlighting the sensitivity of the technique.

Full lengths of "confined" fission tracks were utilized for track length studies in apatite. They are defined as tracks that do not intersect the polished crystal surface but have been etched via other tracks or fractures. In this way, the whole length of track is surely etched, and measured using a digitizing tablet. The device is connected to a microcomputer, super-imposed on the microscope field of view via a projection tube. This system, which is cali-brated against a stage graticule ruled in 2-µm divisions, enables individual tracks to be measured in a precision of ±0.2 µm. Because of anisotropic annealing efficiency of fission tracks residing in apatite [10], we measured tracks only in prismatic grains, which show sharp polishing scratches with well-etched tracks having omnidirectionally narrow cone angle. According to the recommendations of Laslett et al. [11], only horizontal tracks were measured. We measured 100 tracks whenever possible. As for samples with low-track density or those in which only a limited number of apatite grains were obtained, fewer confined tracks may inevitably be available. Hence, the whole mount was scanned in order to find as many confined tracks as possible. A summary of the length measurement of fission tracks is presented in **Table 4**.

Sample number	Mean track length (µm)	Standard deviation (µm)	Number of tracks (N)	Number of tracks in length intervals (µm)																			
				1	2	3	4	5	6	7	8	9	10	11	12	13	14	15	16	17	18	19	20
Outcrop samples																							
GC1181-3	12.77 ± 0.20	2.00	103	–	–	–	–	–	–	3	–	–	4	7	19	17	22	22	8	–	–	1	–
GC1181-4	12.87 ±0.19	1.95	103								2	3	1	5	18	29	16	18	6	3	1	1	–

Track length measurements by: M. Moore for samples 3–4.

Table 4. Summary of length distribution of fission tracks.

3.5. Thermal history interpretation of AFTA data

A compilation of confined track length data in a large number of apatite samples showed that the form of the track length distribution was a sensitive indicator of the style of thermal history [12]. Laboratory studies [10, 13, 14], together with detailed mathematical analysis [11, 15, 16], have established that the reduction in track length causes a reduction in the fission track age, by reducing the proportion of tracks that can intersect a polished grain surface. They demonstrated that as a result of heating, the mean track length is progressively reduced and the tracks effectively "shrink" from each end, until some individual tracks may break up into several segments in the final stages. This realization underpins all subsequent studies involving the quantitative prediction of apatite fission track parameters and the extraction of thermal history information from such data. Laslett et al. [17] showed that the variation of the mean track length with temperature and time can be well described by a "fanning Arrhenius plot" model, in which contours of equal track length reduction form straight lines in a plot of time against inverse absolute temperature, with the slope of these lines (reflecting an "activation energy") increasing as the degree of annealing increases. Their improved definition of the kinetics of fission track annealing obtained by using the mean confined track length as the fundamental parameter, combined with a detailed understanding of the way in which the reduction in track length is manifested in the fission track age [14], provided the basis for making realistic predictions of apatite fission track parameters within usual geological situations.

A key step in this process is the transition from isothermal annealing models to the variable temperature behavior encountered in geological settings [18]. This step provides a way forward by adopting the principle of "equivalent time." It rules that the annealing rate of a track at any given time depends only on its length to which the track has already been reduced and the prevailing temperature, and not upon the history of how the track reached the present length. On these advances, Green et al. [19] developed methods of quantitatively modeling the response of fission tracks in apatite to various styles of thermal history. The basis of the approach is the recognition that track length reduction is the controlling process in determining the AFTA parameters that result from any particular history. Another important finding is that chlorine content exerts a systematic influence on annealing rates [10, 13, 20]. In practical applications of AFTA, variation in fission track age and track length with Cl weight content allows the identification of any anomalous grains that might represent unusual annealing properties (e.g., [21]). Such anomalies can be eliminated from the dataset prior to the extraction of thermal history solutions. In usual geological settings, differential annealing effects for individual samples are maximized in rocks that have been heated to the critical temperatures (typically 90–120°C) where the most sensitive (i.e., low-Cl content) apatite grains are totally annealed, whereas more resistant (i.e., high-Cl content) apatites remain unaffected. Actually, since most common apatites tend to contain less than 0.1 wt% Cl, it should be expected that the apatites analyzed in most published studies might be more sensitive than the Durango apatite that was used in the Laslett et al. [17] model. Thus, it is possible that much of the so-called anomalous Late Cenozoic cooling reported in many studies could be due to such compositional effects, rather than any innate deficiencies in the model [22]. A summary of the AFTA data is shown in **Table 5**.

Sample no. (ID in paper)	Present temp. (°C)	Stratigraphic age (Ma)	Measured mean FT length (μm)	Predicted* mean FT length (μm)	Measured FT age (Ma)	Predicted* FT age (Ma)
GC1181-3 (15040401)	10	71–65	12.77±0.20	14.99	65.9±5.6	70
GC1181-4 (15040402)	10	71–65	12.87±0.19	15.02	84.6±8.3	70

* Values predicted from the default thermal history, that is, assuming that each sample is now at its maximum temperature since deposition. The values refer only to tracks formed after deposition. Samples may contain tracks inherited from sediment provenance areas. Calculations refer to apatites within the measured range of composition for each sample.

Table 5. Summary of AFTA data in two outcrop samples.

3.6. Results of fission track analyses

Basic analytical data for apatite grains separated from Sp. 15040401 and 15040402 are presented in **Figures 2** and **3**, respectively. Both samples analyzed in this study showed unusual and quite distinctive Cl content histograms (**Figures 2B** and **3B**). Detrital apatites from common quartzo-feldspathic sandstones around the world show a typical histogram of Cl contents in which the majority of grains have Cl contents between 0 and 0.1 wt%, while a smaller number of grains give values up to ~0.5 wt% and occasional grains contain 0.5–1.0 wt% Cl.
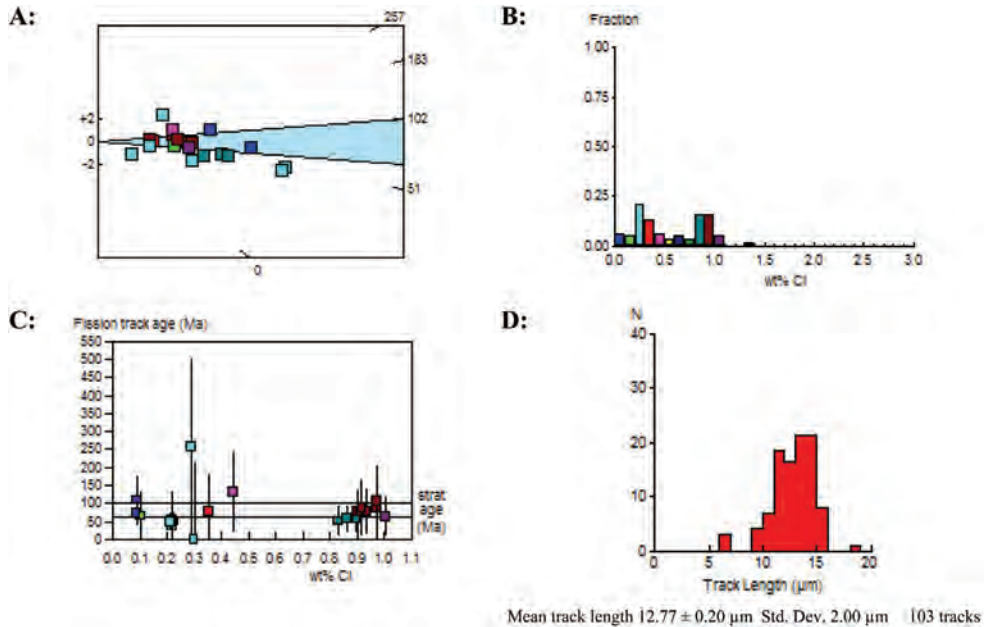

Mean track length 12.77 ± 0.20 μm Std. Dev. 2.00 μm   103 tracks

Figure 2. Fission track age data for Sp. 15040401. A: Radial plot of single grain ages. B: Distribution of Cl contents in apatite grains. C: Single grain age versus weight % Cl for individual apatite grains. D: Distribution of confined track lengths.
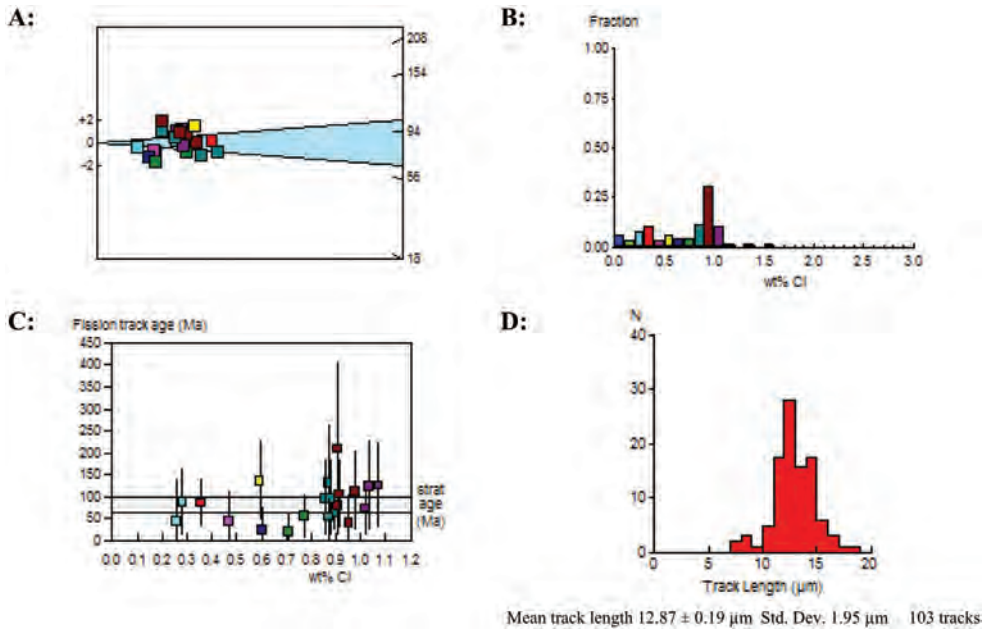
Figure 3. Fission track age data for Sp. 15040402. A: Radial plot of single grain ages. B: Distribution of Cl contents in apatite grains. C: Single grain age versus weight % Cl for individual apatite grains. D: Distribution of confined track lengths.

By contrast, both samples analyzed here showed a broad, bimodal distribution of Cl contents, with prominent peaks at approximately 0.2–0.4 wt% and between 0.8 and 1.0 wt%, with some grains containing as much as 1.5 wt% Cl. Such broad distributions of Cl content are commonly diagnostic of a derivation of apatites from tuffaceous volcanic units. In each of the samples analyzed for this paper, the measured distribution of the compositions has been employed in interpreting the AFTA data, using the methods outlined in the previous section.

In these figures, plots of fission track ages of single apatite grains against Cl content (**Figures 2C** and **3C**) are used to assess the degree of annealing. As an example, grains with a range of Cl contents from zero to some upper limit must have been totally annealed if those with the composition range all yield similar fission track ages that are significantly younger than the stratigraphic age. Or else, the sample displays a high degree of partial annealing in case that the fission track age falls rapidly with decreasing Cl content. As mentioned above, both samples analyzed in the present study showed a broad, bimodal distribution of Cl contents, and the unusual distribution of compositions has been employed in interpreting the AFTA data.

Figure 4 schematically presents the basic concept of the AFTA analysis, which was explained in detail in Section 3.5. Because only a limited number of outcrop samples have been analyzed in the present study, models were constructed for variable paleogeothermal gradients and on the assumption of a long-term constant surface temperature of 10°C. After all the necessary verifications, the thermal history interpretation was obtained for Sp. 15040401 and 15040402, as depicted in **Figures 5** and **6**, respectively.
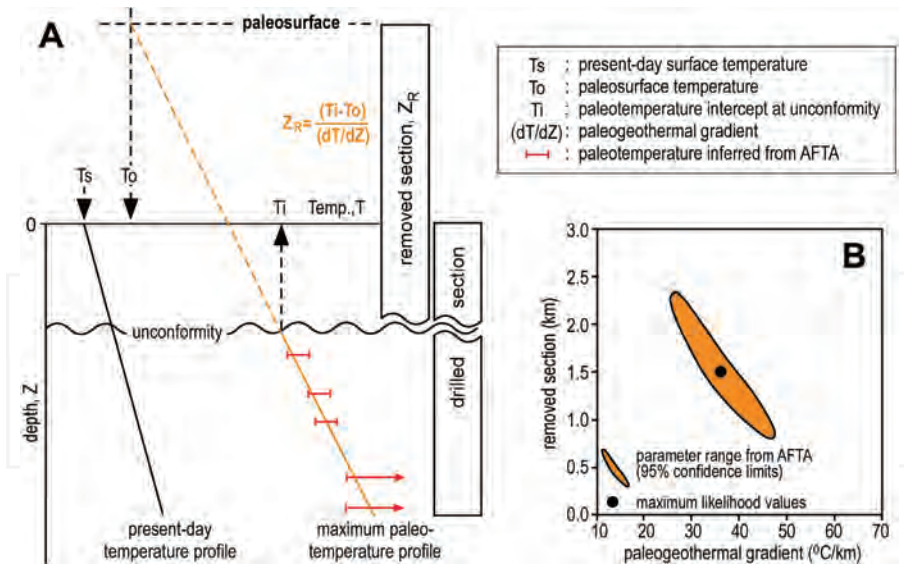
Figure 4. Schematic diagrams showing the AFTA methodology. Heating due to deeper burial (possibly often combined with elevated heat flow) and amounts of exhumation (or deeper burial) can be estimated by fitting a linear paleogeothermal gradient to a series of paleotemperature constraints from subsurface samples. It is then extrapolated to an assumed paleosurface temperature, as shown in a generalized section (A). Note that higher gradients extrapolate to lower values of removed section, while lower gradients correspond to larger amounts of removed section. Statistical analysis allows the definition of the range of values of paleogeothermal gradient and removed section within 95% confidence limits, represented by a hyperbolic ellipsoid in (B).
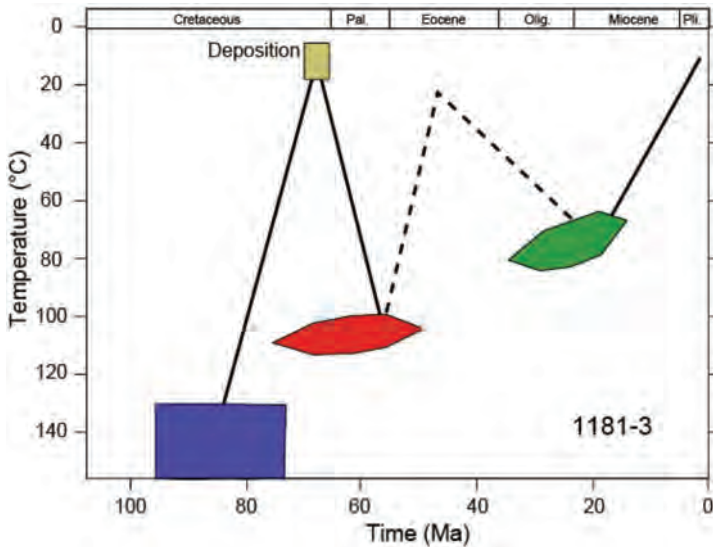

Figure 5. Thermal history interpretation of AFTA data for Sp. 15040401.
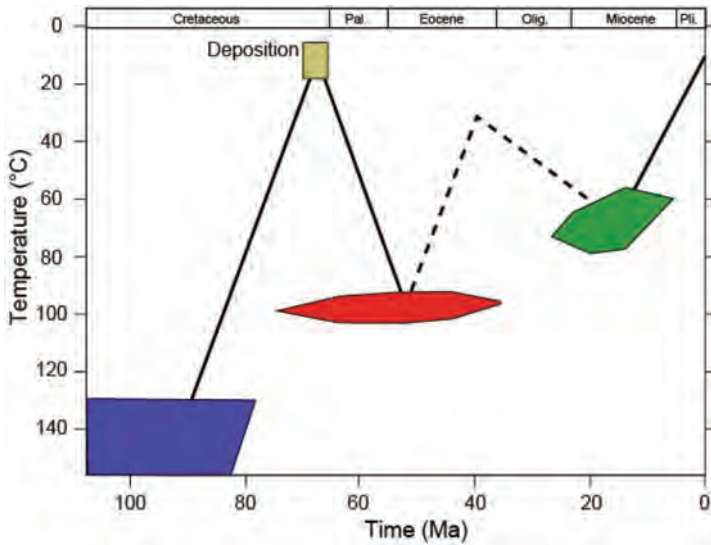
Figure 6. Thermal history interpretation of AFTA data for Sp. 15040402.

In **Figures 5** and **6**, we ran simulations of the data using Geotrack's in-house numerical model of the AFTA system and defined the range of conditions that give predictions consistent with the data with 95% confidence limits as depicted by Green and Duddy [23]. Our analyses have indicated that the evidence of higher temperatures in the past is not obtained from FT ages but instead from track length distribution. Since the effect of Cl contents on the mean track length was quantitatively given by Green and Duddy [24], we employed their result (**Figure 8** of [24]) to construct a self-consistent model.

The ZFTA results for Sp. 15040401 and 15040402 are presented in **Tables 6** and **7**, respectively, and integrated with AFTA results for the thermal history reconstruction detailed in the next section.

GC1181-3 Zircon									15040401	
Counted by: PFG										
Slide ref	Current grain no	N_s	N_i	N_a	ρ_s	ρ_i	RATIO	U (ppm)	FT. AGE (Ma)	
G1269-1	1	53	51	15	5.615E+06	5.403E+06	1.039	215.5	60.6 ±	12.0
G1269-1	2	95	71	27	5.591E+06	4.179E+06	1.338	166.7	77.9 ±	12.4
G1269-1	3	58	44	40	2.304E+06	1.748E+06	1.318	69.7	76.8 ±	15.5
G1269-1	8	189	141	50	6.007E+06	4.481E+06	1.340	178.8	78.1 ±	8.9
G1269-1	9	105	74	20	8.343E+06	5.880E+06	1.419	234.6	82.6 ±	12.7
G1269-1	11	132	147	40	5.244E+06	5.840E+06	0.898	233.0	52.4 ±	6.4
G1269-1	12	101	84	20	8.025E+06	6.674E+06	1.202	266.2	70.1 ±	10.5

Slide ref	Current grain no	N_s	N_i	N_a	ρ_s	ρ_i	RATIO	U (ppm)	FT. AGE (Ma)	

GC1181-3 Zircon ... **15040401**

Counted by: PFG

Slide ref	Current grain no	N_s	N_i	N_a	ρ_s	ρ_i	RATIO	U (ppm)	FT. AGE (Ma)	
G1269-1	13	116	94	25	7.373E+06	5.975E+06	1.234	238.4	71.9 ±	10.1
G1269-1	21	150	151	36	6.621E+06	6.665E+06	0.993	265.9	57.9 ±	6.8
G1269-1	24	93	65	25	5.911E+06	4.132E+06	1.431	164.8	83.3 ±	13.6
G1269-1	25	122	98	40	4.847E+06	3.893E+06	1.245	155.3	72.5 ±	10.0
G1269-1	26	119	95	50	3.782E+06	3.019E+06	1.253	120.4	73.0 ±	10.2
G1269-1	27	119	83	25	7.564E+06	5.276E+06	1.434	210.5	83.5 ±	12.1
G1269-1	33	139	90	25	8.835E+06	5.721E+06	1.544	228.2	89.9 ±	12.3
G1269-1	34	94	84	15	9.958E+06	8.899E+06	1.119	355.0	65.2 ±	9.9
G1269-1	35	111	90	40	4.410E+06	3.575E+06	1.233	142.6	71.9 ±	10.3
G1269-1	37	152	112	40	6.038E+06	4.449E+06	1.357	177.5	79.0 ±	10.0
G1269-1	38	91	68	40	3.615E+06	2.701E+06	1.338	107.8	77.9 ±	12.6
G1269-1	39	97	97	30	5.138E+06	5.138E+06	1.000	205.0	58.3 ±	8.5
G1269-1	41	99	80	30	5.244E+06	4.238E+06	1.237	169.0	72.1 ±	11.0
		2235	1819		5.611E+06	4.566E+06		182.2		

Area of basic unit = 6.293E-07 cm^{-2}

χ^2 = 21.327 with 19 degrees of freedom

$P(\chi^2)$ = 31.9%

Age Dispersion = 6.268% (did not converge)

N_s/N_i = 1.229 ± 0.039

Mean Ratio = 1.249 ± 0.038

Ages calculated using a zeta of 87.7 ± 0.8 for U3 glass

ρ = 1.336E+06cm^{-2} ND=2102

ρ_D interpolated between the top of can;
ρ =1.336E+06cm^{-2} ND=1051

bottom of can; ρ =1.336E+06cm^{-2} ND=1051

POOLED AGE = 71.6±2.8 Ma

CENTRAL AGE= 71.7 ± 3.0 Ma

Table 6. Details of zircon fission track analysis for Sp. 15040401.

GC1181-4 Zircon ... **15040402**

Counted by: PFG

Slide ref	Current grain no	N_s	N_i	N_a	ρ_s	ρ_i	RATIO	U (ppm)	F.T. AGE (Ma)	
G1269-2	2	68	56	20	5.403E+06	4.449E+06	1.214	177.5	70.8 ±	12.9
G1260-2	3	80	57	24	5.297E+06	3.774E+06	1.404	150.6	81.7 ±	14.3
G1269-2	5	69	70	20	5.482E+06	5.562E+06	0.986	221.9	57.5 ±	9.8
G1269-2	9	159	55	25	1.011E+07	3.496E+06	2.891	139.5	167.2 ±	26.5

GC1181-4 Zircon									15040402	
Counted by: PFG										
Slide ref	Current grain no	N_s	N_i	N_a	ρ_s	ρ_i	RATIO	U (ppm)	F.T. AGE (Ma)	
G1269-2	10	75	57	24	4.966E+06	3.774E+06	1.316	150.6	76.6 ±	13.6
G1269-2	12	132	104	20	1.049E+07	8.263E+06	1.269	329.6	73.9 ±	9.9
G1269-2	13	56	79	12	7.416E+06	1.046E+07	0.709	417.3	41.4 ±	7.3
G1269-2	18	122	105	50	3.877E+06	3.337E+06	1.162	133.1	67.7 ±	9.2
G1269-2	19	58	47	16	5.760E+06	4.668E+06	1.234	186.2	71.9 ±	14.2
G1269-2	21	40	38	18	3.531E+06	3.355E+06	1.053	133.8	61.4 ±	14.0
G1269-2	22	80	46	24	5.297E+06	3.046E+06	1.739	121.5	101.1 ±	18.9
G1269-2	24	97	90	40	3.853E+06	3.575E+06	1.078	142.6	62.8 ±	9.3
G1269-2	30	126	102	50	4.004E+06	3.242E+06	1.235	129.3	72.0 ±	9.7
G1269-2	32	48	54	24	3.178E+06	3.575E+06	0.889	142.6	51.9 ±	10.4
G1269-2	33	82	80	16	8.144E+06	7.945E+06	1.025	317.0	59.8 ±	9.5
G1269-2	35	79	54	50	2.511E+06	1.716E+06	1.463	68.5	85.1 ±	15.2
G1269-2	36	54	36	18	4.767E+06	3.178E+06	1.500	126.8	87.3 ±	18.9
G1269-2	40	67	63	16	6.654E+06	6.257E+06	1.063	249.6	62.0 ±	11.0
G1269-2	46	84	65	30	4.449E+06	3.443E+06	1.292	137.3	75.3 ±	12.6
G1269-2	48	55	58	50	1.748E+06	1.843E+06	0.948	73.5	55.3 ±	10.5
		1631	1316		4.738E+06	3.823E+06		152.5		

Area of basic unit = 6.293E-07 cm⁻²

Ages calculated using a zeta of 87.7 ± 0.8 for U3 glass

χ^2 = 58.002 with 19 degrees of freedom

ρ = 1.336E+06cm⁻² ND = 2102

$P(\chi^2)$=0.0%

ρ_D interpolated between the top of can; ρ = 1.336E+06cm⁻² ND=1051

Age dispersion =22.242%

Bottom of can; ρ = 1.336E+06cm⁻² ND = 1051

N_s/N_i= 1.239 ± 0.046

POOLED AGE = 72.2 ± 3.2 Ma

Mean ratio = 1.274 ± 0.100

CENTRAL AGE = 71.1 ± 4.8 Ma

Table 7. Details of zircon fission track analysis for Sp. 15040402.

4. Discussion

The thermal history interpretation of AFTA data for two outcrop samples suggested three cooling (i.e., uplift) events around the study area. Among them, the Cenomanian–Campanian cooling from >130°C in the earliest of three episodes predates the deposition of the host sand-

stones, and appears to reflect a different provenance for the apatites compared to zircons. The Campanian–middle Eocene and late Oligocene–late Miocene cooling episodes clearly postdate the deposition of host rocks. Paleotemperatures in these episodes are interpreted as being due to deeper burial prior to cooling as a result of exhumation (uplift and erosion). Assuming a paleogeothermal gradient of 30°C/km, paleotemperatures of approximately 100°C prior to Campanian–middle Eocene cooling correspond to burial by ~3 km of section. Similarly, paleotemperatures around 70°C prior to late Oligocene–late Miocene cooling correspond to burial by ~2 km of section.

ZFTA data define cooling from >300°C at ca. 70 Ma, whereas AFTA data define an initial phase of cooling from >130°C that began in the interval of 95–78 Ma. This difference between the timing determined using the two techniques appears to indicate the different provenances of the two minerals, as indicated above.

Radiometric dates reported from the hinterlands seem to support the above-mentioned hypothesis of distinct provenances. **Figure 7** presents reliable radiometric ages obtained from the Cretaceous igneous rocks distributed in the central part of southwest Japan [25]. The ages show an explicit bimodal distribution, which agrees with the results of the present study. Although the previous dataset includes varied methods with different closing temperatures,
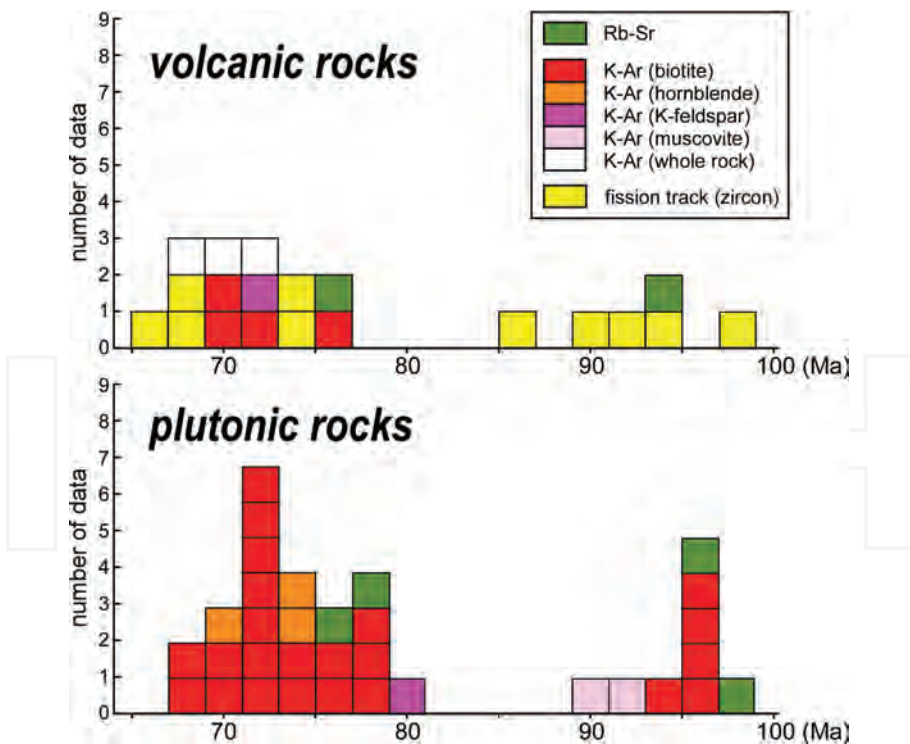

Figure 7. Histogram of radiometric ages reported from the Cretaceous igneous rocks distributed in the central part of southwest Japan [25].

ages obtained using the same technique and mineral (e.g., K–Ar ages on biotite) show clearly two peaks. Thus, the multiple igneous events on the Cretaceous Eurasian margin have been confirmed through the present AFTA and ZFTA analyses.

Figure 8 presents a complete reconstruction of the thermal history derived from AFTA and ZFTA analyses. As mentioned above, the present study has indicated distinct Cretaceous provenances for apatite and zircon grains yielded from outcrop sandstones of the Izumi Group. The second episode from the Campanian to the middle Eocene appears to correspond to a stage of regional uplift identified on the forearc of the northeastern Japan arc [26] although its driving force and/or effective area should be assessed through further study. The tectonic context of the youngest cooling (uplift) event terminated around the end of Miocene is intriguing. Based on their seismic interpretation on the backarc shelf of southwest Japan, Itoh and Nagasaki [27] argued that an arc contraction event at the timing had a regional impact under prevailing north–south tectonic stress probably because of the resumed convergence of the Philippine Sea Plate. In other words, younger deformation phases or shear heating linked to recent dextral slips on the MTL active fault system had no significant effect on the annealing of fission tracks in rock-forming minerals.
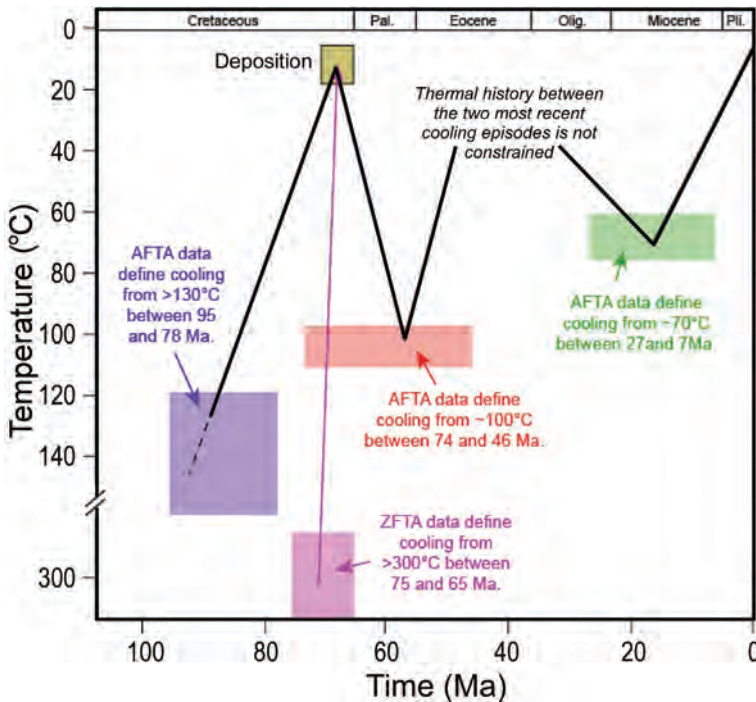

Figure 8. Preferred thermal history reconstruction of AFTA and ZFTA data in two outcrop sandstones of the Izumi Group in southwest Japan. As for the apatite analysis, thermal events were not supposed by FT ages but by track length distribution. As for the zircon analysis, the range of the cooling interval (75–65 Ma) was given as two sigma uncertainties on the weighted mean age.

Our research revealed a timeline of thermal episodes on the MTL. Because the fault has a quite long active trace, it is plausible that different tectonic history is applicable to remote segments of the MTL. Based on a systematic FT thermochronology, Tagami et al. [28] stated that thermal overprinting events adjacent to the eastern part of the MTL may be likely due to shear heating upon the fault during the Oligocene and Miocene. As presented in the geochemistry paper in this book (Chapter 6 by Kaneko et al.), the eastern portion of the longstanding fault may have evolved through different path from its central portion.

5. Conclusions

(1) Excellent yields of apatite and zircon were obtained from two sandstone samples of the Izumi Group along the MTL active fault system, resulting in very high-quality AFTA and ZFTA data, and the interpretations made in this study are regarded as highly reliable.

(2) AFTA data in both samples define three episodes of cooling from elevated paleotemperatures. If the results in both samples represent the effects of the same events, then the AFTA data define cooling that began in the following intervals:

95–78 Ma: Cenomanian–Campanian, from >130°C.

74–46 Ma: Campanian–middle Eocene, from ~100°C.

27–7 Ma: late Oligocene–late Miocene, from ~70°C.

(3) ZFTA data in the two samples are highly consistent, as are the AFTA data. These results suggest that no significant fault offsets exist between the two samples.

(4) ZFTA data suggest that the zircon grains cooled below ~250–300°C between 75 and 65 Ma. This interval overlaps the Maastrichtian depositional age range (71–65 Ma) for the sandstones, suggesting a rapidly cooled provenance contemporaneous with deposition.

(5) Cenomanian–Campanian cooling from >130°C in the earliest of the three episodes predates the deposition of the host sandstones, and appears to reflect a different provenance for the apatites than for the zircons. The Campanian–middle Eocene and late Oligocene–late Miocene-cooling episodes clearly postdate the deposition of the host sandstones. The paleotemperatures in these episodes were interpreted as being due to deeper burial prior to cooling as a result of exhumation (uplift and erosion). Assuming a paleogeothermal gradient of 30°C/km, paleotemperatures around 100°C prior to Campanian–middle Eocene cooling correspond to burial by ~3 km of section. Similarly, paleotemperatures of approximately 70°C prior to late Oligocene–late Miocene cooling correspond to burial by ~2 km of section.

(6) ZFTA data define cooling from >300°C at around 70 Ma, whereas AFTA data define an initial phase of cooling from >130°C that began in the interval of 95–78 Ma. This difference in the timing determined using the two techniques appears to indicate the different provenances of the two minerals, as indicated above.

(7) Radiometric dates reported from the hinterlands appear to support the hypothesis of distinct provenances. Cretaceous igneous rocks distributed within the central part of southwest Japan yielded ages showing an explicit bimodal distribution, which agrees with the results of the present AFTA and ZFTA analyses. Ages obtained using the same technique and mineral (e.g., K–Ar ages on biotite) show clearly two peaks and support the occurrence of multiple igneous events on the Cretaceous Eurasian margin.

(8) The second and third thermal episodes from the Campanian to the middle Eocene and from the late Oligocene to the late Miocene correspond, respectively, to stages of regional uplift identified around the forearc of northeast Japan and a strong arc contraction event under a prevalent north–south tectonic stress caused by resumed northerly convergence of the Philippine Sea Plate. The latest cooling (i.e., uplift) event also indicates that the Quaternary deformation phases or shear heating linked to vigorous dextral slips on the MTL active fault system had no significant effect on the annealing of fission tracks in rock-forming minerals in the fault-adjoining localities.

Acknowledgements

Author details

Yasuto Itoh[1]*, Paul F. Green[2], Keiji Takemura[3] and Tomotaka Iwata[4]

*Address all correspondence to: yasutokov@yahoo.co.jp

1 Graduate School of Science, Osaka Prefecture University, Osaka, Japan

2 Geotrack International, Brunswick West, VIC, Australia

3 Institute for Geothermal Sciences, Kyoto University, Beppu, Japan

4 Disaster Prevention Research Institute, Kyoto University, Uji, Japan

References

[1] Itoh Y, Uno K, Arato H. Seismic evidence of divergent rifting and subsequent deformation in the southern Japan Sea, and a Cenozoic tectonic synthesis of the eastern Eurasian margin. Journal of Asian Earth Sciences. 2006; 27: 933-942.

[2] Makimoto H, Miyata T, Mizuno K, Sangawa A. Geology of the Kokawa District, with Geological Sheet Map at 1:50,000. Tsukuba: Geological Survey of Japan, AIST; 2004. 89 p.

[3] Tanaka J. Sedimentary facies of the Cretaceous Izumi turbidite system, southwest Japan - an example of turbidite sedimentation in an elongated strike-slip tectonic basin. Journal of the Geological Society of Japan. 1989; 95: 119-128.

[4] Hurford AJ, Green PF. The zeta age calibration of fission track dating. Isotope Geoscience. 1983; 1: 285-317.

[5] Gleadow AJW. Fission track dating methods: what are the real alternatives? Nuclear Tracks. 1981; 5: 3-14.

[6] Wagner GA, Reimer GM. Fission track tectonics: the tectonic interpretation of fission track ages. Earth and Planetary Science Letters. 1972; 14: 263-268.

[7] Naeser CW, Forbes RB. Variation of fission track ages with depth in two deep drill holes. EOS (abstract). 1976; 57: 363.

[8] Bhandari N, Bhat SG, Lal D, Rajagopalan G, Tamhane AS, Venkatavaradan VS. Fission fragment tracks in apatite: recordable track lengths. Earth and Planetary Science Letters. 1971; 13: 191-199.

[9] Green PF. On the cause of the shortening of spontaneous fission tracks in certain minerals. Nuclear Tracks. 1980; 4: 91-100.

[10] Green PF, Duddy IR, Gleadow AJW, Tingate PR, Laslett GM. Thermal annealing of fission tracks in apatite 1. A qualitative description. Chemical Geology (Isotope Geoscience Section). 1986; 59: 237-253.

[11] Laslett GM, Kendall WS, Gleadow AJW, Duddy IR. Bias in measurement of fission track length distributions. Nuclear Tracks. 1982; 6: 79-85.

[12] Gleadow AJW, Duddy IR, Green PF, Lovering JF. Confined fission track lengths in apatite—a diagnostic tool for thermal history analysis. Contributions to Mineralogy and Petrology. 1986; 94: 405-415.

[13] Green PF, Duddy IR, Gleadow AJW, Tingate PR, Laslett GM. Fission-track annealing in apatite: track length measurements and the form of the Arrhenius plot. Nuclear Tracks. 1985; 10: 323-328.

[14] Green PF. The relationship between track shortening and fission track age reduction in apatite: combined influences of inherent instability, annealing anisotropy, length bias and system calibration. Earth and Planetary Science Letters. 1988; 89: 335-352.

[15] Galbraith RF, Laslett GM. Some calculations relevant to the thermal annealing of fission tracks in apatite. Proceedings of the Royal Society, London. 1988; A419: 305-321.

[16] Galbraith RF, Laslett GM. Apatite fission track analysis: geological thermal history analysis based on a three-dimensional random process of linear radiation damage. Philosophical Transcripts of the Royal Society of London. 1990; 332: 419-438.

[17] Laslett GM, Green PF, Duddy IR, Gleadow AJW. Thermal annealing of fission tracks in apatite 2. A quantitative analysis. Chemical Geology (Isotope Geoscience Section). 1987; 65: 1-13.

[18] Duddy IR, Green PF, Laslett GM. Thermal annealing of fission tracks in apatite 3. Variable temperature behaviour. Chemical Geology (Isotope Geoscience Section). 1988; 73: 25-38.

[19] Green PF, Duddy IR, Laslett GM, Hegarty KA, Gleadow AJW, Lovering JF. Thermal annealing of fission tracks in apatite 4. Quantitative modelling techniques and extension to geological timescales. Chemical Geology (Isotope Geoscience Section). 1989; 79: 155-182.

[20] Gleadow AJW, Duddy IR. Fission track analysis: a new tool for the evaluation of thermal histories and hydrocarbon potential. APEA Journal. 1981; 23: 93-102.

[21] Crowhurst PV, Green PF, Kamp PJJ. Appraisal of (U-Th)/He apatite thermochronology as a thermal history tool for hydrocarbon exploration: an example from the Taranaki Basin, New Zealand. AAPG Bulletin. 2002; 86: 1801-1819.

[22] Green P. The importance of validating annealing models (abstract). In: Proceedings of 10th International Conference on Fission Track Dating and Thermochronology; Amsterdam. 2004. p. 53.

[23] Green PF, Duddy IR. Synchronous exhumation events around the Arctic including examples from Barents Sea and Alaska North Slope. In: Vining BA, Pickering SC, editors. Petroleum Geology, From Mature Basins to New Frontiers. Proceedings of the 7th Petroleum Geology Conference. London: The Geological Society; 2010. pp. 633-644. DOI: 10.1144/0070633

[24] Green PF, Duddy IR. Thermal history reconstruction in sedimentary basins using apatite fission-track analysis and related techniques. In: Analyzing the Thermal History of Sedimentary Basins - Methods and Case Studies. SEPM (Society for Sedimentary Geology); 2012. pp. 65-104.

[25] Matsuura H, Kurimoto C, Sangawa A, Bunno M. Geology of the Hirone District, with Geological Sheet Map at 1:50,000. Tsukuba: Geological Survey of Japan, AIST; 1995. 110 p.

[26] Takano O. Variation in forearc basin configuration and basin-filling depositional systems as a function of trench slope break development and strike-slip movement: examples from the Cenozoic Ishikari-Sanriku-oki and Tokai-oki-Kumano-nada forearc basins, Japan. In: Itoh Y, editor. Mechanism of Sedimentary Basin Formation-Multidisciplinary Approach on Active Plate Margins. Rijeka: InTech; 2013. http://dx.doi.org/10.5772/56751

[27] Itoh Y, Nagasaki Y. Crustal shortening of Southwest Japan in the Late Miocene. The Island Arc. 1996; 5: 337-353.

[28] Tagami T, Lal N, Sorkhabi RB, Nishimura S. Fission track thermochronologic analysis of the Ryoke belt and the Median Tectonic Line, southwest Japan. Journal of Geophysical Research. 1988; 93: 13705-13715.